doi:10.1016/j.corsci.2009.06.001

Microstructural characterization of Ru-doped NiCoCrAlYTa coupons treated by thermal oxidation

F. Juárez L [a,*], C. Vahlas [b], J.A. Alvarez C [a]

[a] CIITEC-IPN 02250, Cerrada de Cecati S/N, Santa Catarina Azcapotzalco, 002250 México DF, Mexico
[b] CIRIMAT UMR 5085, ENSIACET, 118 Route de Narbonne, 31077 Toulouse cedex 4, France

A B S T R A C T

Isothermal oxidation of sintered Ru-doped and undoped Ni-alloy coupons in the range of 1173–1423 K was investigated. To assess the effect of Ruthenium doping, microstructural characterization was performed to compare the samples before and after oxidation treatment at 1173 K. Furthermore, cyclic oxidation tests on the Ru-doped and undoped coupons were carried out in a thermogravimetry apparatus at 1223 and 1323 K. The addition of 0.8 wt.% of Ru in NiCoCrAlYTa powders sintered coupons does not degrade the material's resistance to oxidation conditions.

Keywords:
A. Superalloys
B. Thermal cycling, SEM
C. Oxidation

1. Introduction

It is important for novel aerospace applications, to improve the oxidation and corrosion resistance of the protective bond coat of turbine blades operating at elevated temperature, and to increase the adhesion between the bond coat and the adjacent materials, i.e., the substrate and the external thermal barrier. To meet these requirements, doping of nickel aluminide and of MCrAlY (M = Fe, Ni and/or Co) bond coats by various metals or rare earth elements has been studied. It has been found, for example, that addition of rhenium [1] or platinum group metals, namely platinum itself, palladium and ruthenium, improve the mechanical properties of the bond coat and increase the lifetime of appropriate-quality alumina scale that are in contact with the ceramic top coat [2–4]. Thus the presence of these two elements facilitates the hardening of the γ phase, and the coalescence of the precipitates slows down γ [5]. The effect of weak additions of Re on the MCrAlY powders is further documented [6,7]. It has been shown [1] that additions of Re diminish the activity of aluminum in the coating, which would support the formation of the α-Al_2O_3 variety. Specific results concerning the addition of Pt in MCrAlY powders indicate that this decreases the thermal dilation coefficient, moderately increases the elastic limit and ductility and makes possible to increase the lifetime of the scale of Al_2O_3 [8].

The process being investigated here is the superficial doping of commercial powders with platinum group metals and other elements using the spouted-bed metal–organic chemical vapor deposition (SB-MOCVD) technique [9]. Initial results introducing the process were presented in [10–12]. The present work is devoted to the thermal oxidation behavior of sintered ruthenium (Ru-doped) coupons obtained by spouted-bed MOCVD and hot uniaxial pressure. The choice of Ru for this study is based on results previously obtained, in which doping of monocrystalline nickel superalloys with this element reduces their high-temperature creep [13]

* Corresponding author. Tel.:+52 5949572191; fax: +52 57296000.
E-mail addresses: fjuarezl@ipn.mx, fjuarezl681209@yahoo.com.mx (F. Juárez L).

To examine oxidation in greater details, an experiment was carried on Ru-doped coupon surface. Several zones were marked by indentation using a Knoop microhardness test setup. The orientation and relative positions of these zones were identified using micrometric displacements on the turntable of a Scanning Electron Microscopy (SEM). The coupon is oxidized at 1173 K for 1 h in dry air. Microstructural analysis was performed on the marked locations using SEM, EDX, and X-ray diffraction.

Furthermore, to observe the effect of doping on improving the resistance to oxidation at high-temperature, Ru-doped and undoped sintered coupons were sliced and polished. Then, cyclic oxidation tests were carried at stage temperatures of 1223 and 1323 K under dry air of laboratory.

Scanning electron microscopy (SEM), X-ray dispersive spectroscopy (EDS), and X-ray diffraction at grazing incidence (GIXRD), were used for morphological analysis on the microstructure and composition of both sintered Ru-doped samples and oxide scales. Finally secondary ion mass spectrometry (SIMS; CAMECA IMS4F/6F) in imaging mode with O^{2+} primary ions were used for morphologic and microstructural analysis of the sintered Ru-doped samples.

3. Results and discussion

3.1. Isothermal oxidation and microstructural analysis

Fig. 1 presents the mass gain per unit area curves at the four temperatures investigated for the undoped and doped samples.

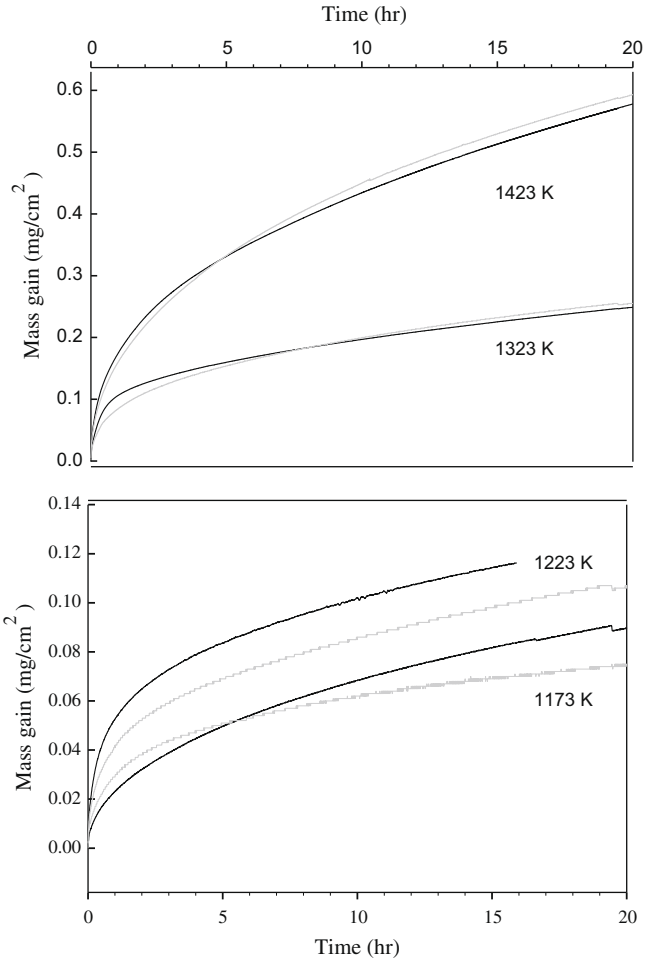

Fig. 1. Mass gain versus oxidation time at 1173 and 1223 (lower part), and 1323, 1423 K (upper part); Ru-doped (black lines) and undoped coupons (gray lines).

The mass gain per unit area after 20 h ranges between 0.07 and 0.6 mg/cm^2, corresponding to a pure, compact alumina thickness of 0.4 and 3 μm, respectively. At all temperatures studied, a transient stage of faster oxidation kinetics can be observed during the initial period of the heat treatment. Curves appear to be very similar for doped and undoped materials, especially at 1323 and 1423 K, where α-alumina is expected to be predominant in the oxide scale. Scale growth kinetic was interpreted using the most general expression for parabolic kinetics:

$$t = a + b\Delta m + c\Delta m^2 \quad (1)$$

where t is the time (s) and Δm is the mass gain per unit area (mg cm^{-2}). Coefficient c is equal to the reciprocal of the parabolic rate constant k_p (mg^2 cm^{-4} s^{-1}) independent of the initial conditions for integration of the rate equation. Eq. (1) was fitted to a small first part (first hour) of the set of (t, Δm) data representative of the initial formation of scale on the surface of the coupons to determine the corresponding k_p values. This equation was also applied to the subsequent range (1–20 h) of the (t, Δm) data to obtain the stationary state value of k_p. The results are presented in an Arrhenius plot in Fig. 2, where variations with temperature of the values of transient and stationary k_p are reported. This diagram confirms the previously reported kinetic behaviour. The transient oxidation kinetics is approximately one order of magnitude higher than the stationary oxidation kinetics at 1223 K. The values reported for k_p in the transient state are in very good agreement with the results of Brumm and Grabke for NiAl oxidation in conditions where transient (theta) alumina is formed [14].

Ru-doped sample behaviour at 1173 K has a slightly different trend as revealed in this (k_p) figure, possibly due to some artefact concerning the heat treatment of the coupon (During MOCVD doped).

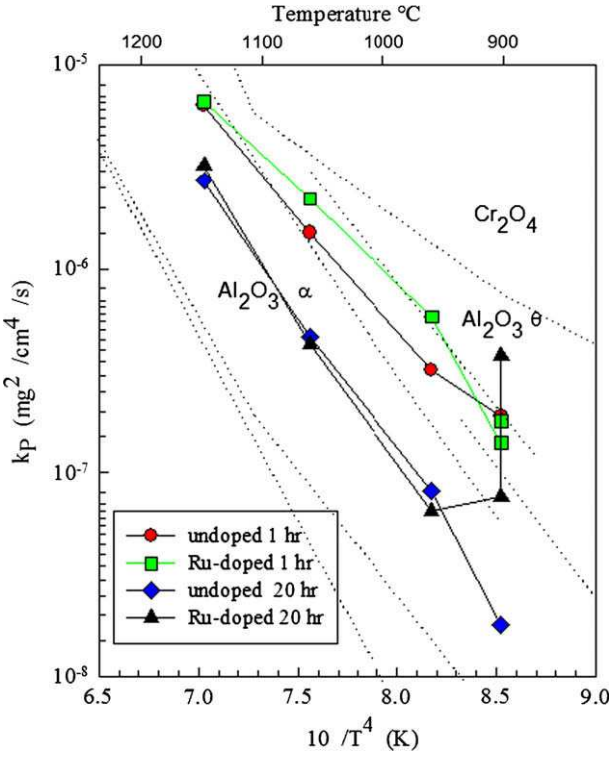

Fig. 2. Arrhenius plots of the parabolic rate constants for the oxidation of the undoped (circles) and Ru-doped (squares) samples, for oxidation times of 1 h (gray symbols) and 20 h (black symbols). Long dash lines mains area from grown of alumina.

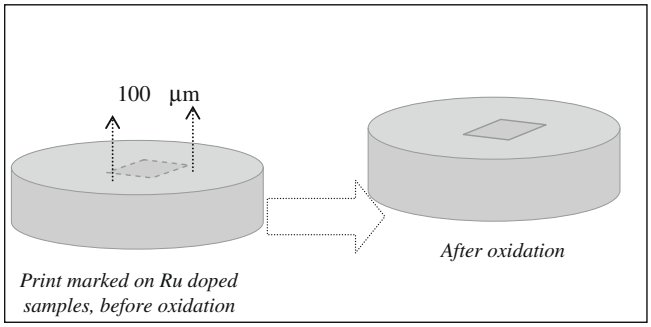

Fig. 3. Experimental protocol followed for the study of the Ru-doped surface (relationship of solids phases alloy and oxides formed).

Several zones were delimited by indentation using a Knoop microhardness indenter. Fig. 3, illustrates the experimental protocol followed for the study on surface of solid phases alloy and the oxides formed.

It was expected to observe that different solid phase induced different behaviors in oxidation [15]. Fig. 4 shows an ensemble from several zones before oxidation (marks) and after oxidation, measured on same points on the Ru-doped sample.

EDS Microanalysis is presented (Fig. 4). According to the lectures, Al concentration is present in the β phase, which is in agreement with dark areas in the backscattered electron SEM micrograph. However, Ru signal was to weak for EDS to establish a elemental map.

It appears as well that the clearest oxide is formed at the equilibrium areas or at inter-phases where they are already characterized by clear contrast. The darkest areas correspond to oxide formed from β phase and light areas correspond to oxides formed over γ phase. By comparing several zones we found interest behaviour and clear relationship between the nature of the solids phases and the scale oxides. Clear areas correspond to the formation of nickel-rich oxide, which can be attributed to NiO oxide detected by X-ray diffraction shown in Fig. 5.

X-ray diffraction analysis shows that the two major oxides are α alumina oxide layer and probably other type of spinel oxides structure of solid solution formed by (Ni, Co)(Al, $Cr)_2O_4$. Thickness of oxide is very thin, according to observations of the very intense diffraction peaks of β and γ phases alloy matrix.

3.2. Cyclic oxidation and microstructural analysis of the products of oxidation

Cyclic oxidation tests were carried out at temperatures 1223 and 1323 K under dry air for Ru-doped and undoped samples. In Fig. 6, the results were plotted in terms of mass gain versus numbers of cycles. As a comparison, a sample of superalloy MCrAlY produced by VPS (vacuum plasma spray) was treated under the same conditions of temperature and dry air. Parabolic behavior was obtained of the mass gain in function of time during cyclic oxidation. Due to inherent error by successive weighting, these curves are more irregular than those obtained by isothermal oxidation.

That behavior at the end of plots curves in undoped coupons could be result of the damage of the coat oxide, which would

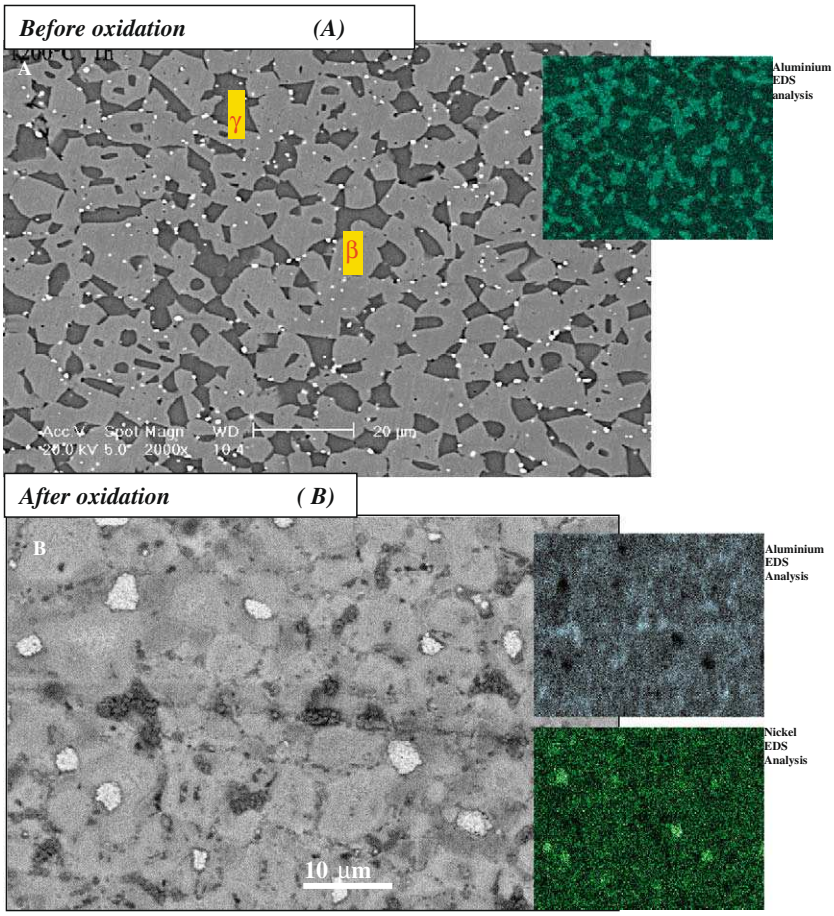

Fig. 4. Assemblage illustrating the state of the surface of Ru-doped sintered sample, polished to 3 µm, before and after isothermal oxidation at 1173 K. Before oxidation (A): SEM Backscattered electron micrograph (high), Al EDS map (high left). After oxidation (B): SEM backscattered electron image (low). Ni and Al EDS map (low left).

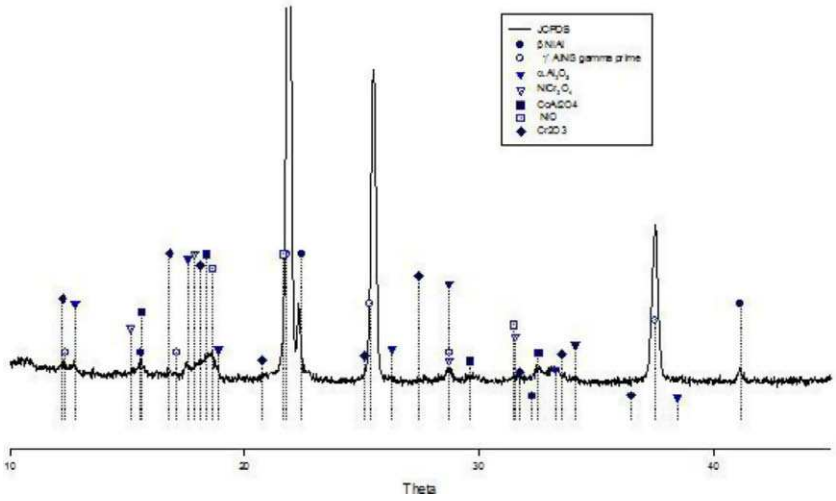

Fig. 5. X-ray diffraction analysis of the Ru-doped samples treatment at 1173 K and 1 h.

become be less protective. In contrast, Ru-doped samples shows negligible trend to form oxide layer, which could be attributed to the presence of Ru.

The comparison between Ru-doped sample and that produced by VPS revealed similar behavior. VPS sample shows mass loss beyond 550 cycles, probably caused by a chipping and followed by separation of the oxide formed. Ru-doped sample shows comparable behavior beyond 650 cycles. Loss mass was calculated on both Ru-doped and undoped samples of 0.4 mg/cm^2 and 0.6 mg/cm^2, respectively. X-ray diffraction of Ru-doped sample after cyclic oxidation at 1323 K shows scale oxide formed to be mainly α alumina and a mix spinel (Ni, Co)(Al, Cr)O_4.

Fig. 7a illustrates the morphological aspect of the oxide formed from undoped sample after cyclic oxidation at 1323 K. It is observed, a negligible chipping developed at sample edge, approximately at the suspension hole, and the general aspect of scale is uniform. In contrast to the tests of isothermal oxidation (short duration), non-influence of the microstructure alloy was observed. This is probably due to the consumption of aluminum from γ phase. Adhered scale oxide is majorly composed of two types of different oxides; one oxide consists of morphology seems to "pink of sands", this is characteristic of transition alumina, which is similarly observed during isothermal oxidation. We expect larger amount δ transient alumina to be present; however, X-ray diffraction does not reveal the presence of δ alumina. We hypothesize that these transient alumina are formed during of first's stages of cyclic oxidation, and subsequently transformed into α stable alumina while preserving their morphology. One other oxide is characterized by regular and smooth, probably α alumina which was formed at the start of oxidation.

Micrograph from Ru-doped and undoped, Fig. 7b shows that the oxide scale formed at 1323 K has a quite different morphology. First of all, spallation was not observed on the Ru-doped surface sample. Morphology of the scale oxide has aspect similar to α and γ phases corresponding to the matrix alloy (principal). Mass gain measured corresponds to a 3 μm scale oxide thickness. The persistence of this microstructure can be the result of the transitory stage, with the formation of an α alumina scale, this formation raise up controlled by anionic diffusion, which would make it possible to preserve the original oxide morphology.

In addition, Fig. 8 illustrates Scanning SIMS maps Al^{27} and Ru^{99} of the same 50 × 50 mm^2 area of a surface polished from Ru-doped sample. Two phases were identified dark and gray on the surfaces. These correspond well to β-NiAl and γ-Ni solid phases, respectively. From a comparison of the two maps, it appears that Ru is present in β-NiAl. This observation could be result of the enhanced plasticity of β-NiAl during the sintering conditions, and agrees with literature reporting that platinum group metals show a remarkable affinity for this phase [3].

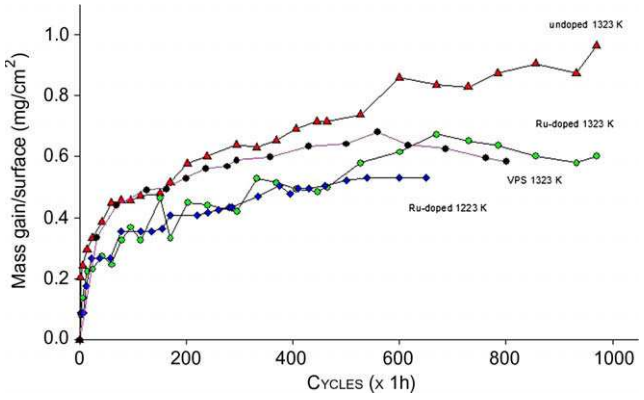

Fig. 6. Mass gain versus time duration cyclic oxidation: cyclic oxidation at 1223 and 1323 K Ru of both Ru-doped and undoped samples. Further VPS sample.

4. Conclusions

Isothermal oxidation of undoped and Ru-doped samples allowed us to investigate the transient and stationary oxidation kinetics in the range 1173–1473 K. Ru doping by MOCVD does not significantly degrade the oxidation behaviour of the NiCoCrAlYTa sintered samples.

SEM characterization of the sintered Ru-doped coupons and oxidized at 1173 k was investigated. This characterization revealed exact relationship between the scale oxides and the matrix alloy microstructure. A thin film of α alumina oxide was formed from β-NiAl, Al-rich zones, and a spinel mixed (Ni, Co)(Al, Cr)$_2O_4$ from γ Ni-rich zones.

Finally, the addition of Ruthenium (0.8% mass) in NiCoCrAlYTa samples reveal a superior behavior under conditions of cyclic oxidation to that of the bond coat produced by VPS. This approach could be extended to study other elements such as Ir, Re, etc. applied to the vanes or turbine.

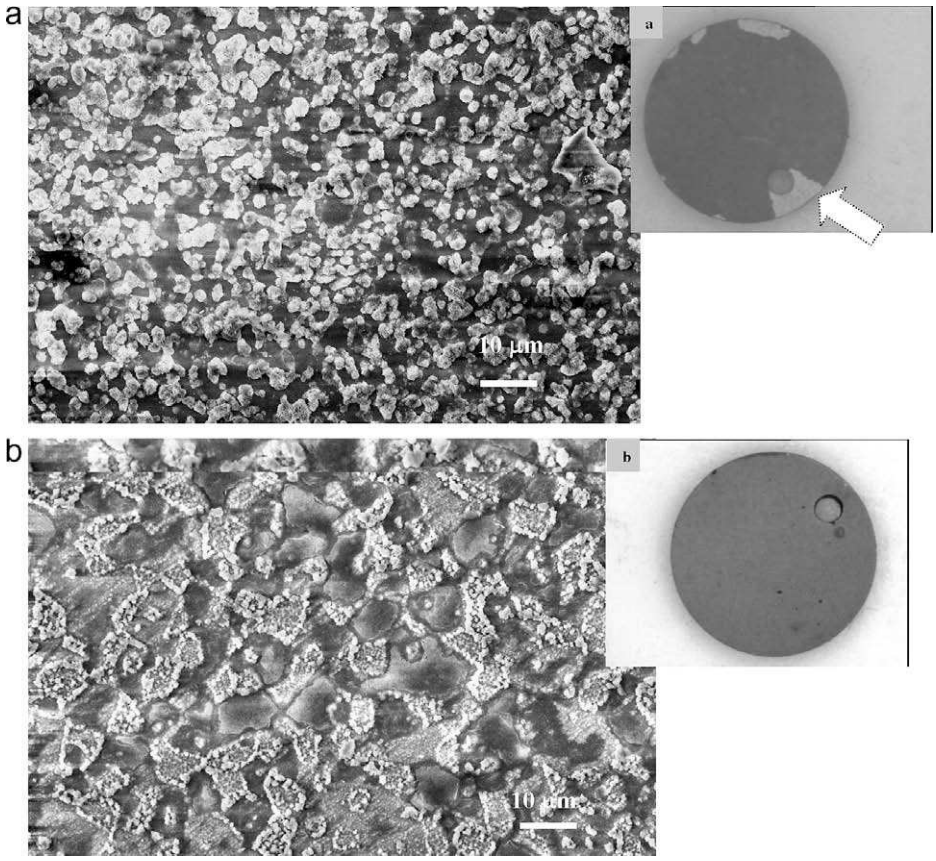

Fig. 7. Samples after cyclic oxidation at 1323 K: undoped; (a) Zone spallation (high left), and detail of oxide layer. Ru-doped; (b) Detail of oxide layer (low).

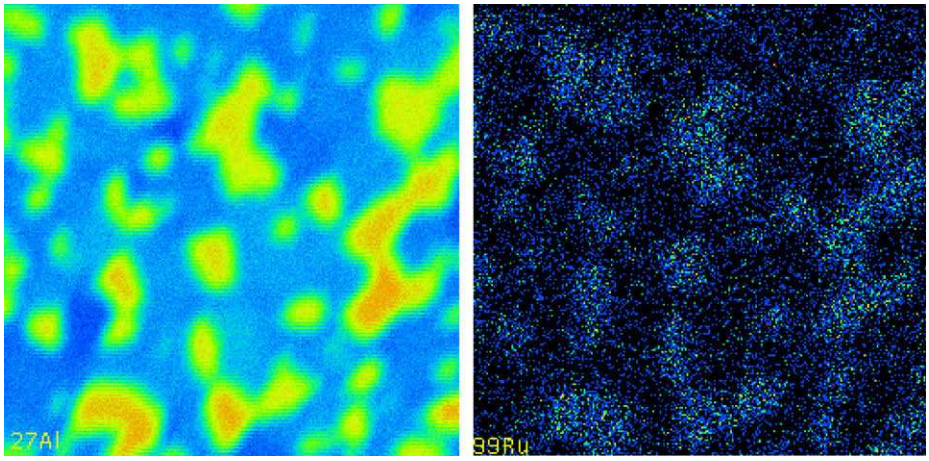

Fig. 8. ^{27}Al and Ru SIMS maps of the same $50 \times 50\ \mu m^2$ area from Ru-doped sample.

Acknowledgements

We are grateful for the support of CIITEC-IPN, México accorded to Fernando Juarez L., with the administrative support of both SIP-COFAA-IPN-México and SNI-CONACyT. The support of the Institute National Polytechnic de Toulouse initiative is also acknowledged.

References

[1] N. Czech, F. Schmitz, W. Stamm, Surf. Coat. Technol. 17 (1994) 68–69.
[2] I.M. Wolff, L.E. Iorio, T. Rumpf, P.V.T. Scheers, J.H. Potgieter, Mater. Sci. Eng. A 241 (1998) 264–276.
[3] S.A. Alperine, P. Josso, J.P. Fournes, J.L. Leger, A.H.L. Malie, D.G. Manesse, EP Patent 0792948 A1, 1997.
[4] T.A. Taylor, D.E. Bettridge. R.C. Tucker, US Patent 5455119, 1995.
[5] R.W. Smashey, C.S. Wukusick, USA, 2 254 651 Accession (2 254 651), 1975.
[6] N. Czech, F. Schmitz, USA, 5 154 885 Accession (5 154 885), 1992.
[7] N. Czech, F. Schmtiz, Patent, USA, 5 268 238 Accession (5 268 238), 1993.
[8] T.A. Taylor, D.E. Bettridge, Surf. Coat. Technol. 86–87 (1996) 9–14.
[9] F. Juarez, A. Castillo, B. Pieraggi, C. Vahlas, J. Phys. IV 11 (2001) 1117–1123.
[10] C. Vahlas, F. Juarez, R. Feurer, P. Serp, B. Caussat, Adv. Mater. CVD 8 (4) (2002) 127–143.
[11] F. Juarez, D. Monceau, D. Tetard, B. Pieraggi, C. Vahlas, Surf. Coat. Technol. 163–164 (2003) 44–49.
[12] M.-C. Lafont, L. Fernando Juáre, C. Vahlas, Scripta Mater. (51) (2004) 699–703.
[13] P. Caron, S. Naveos, J.-L. Raffestin, EP Patent 0971041, 2000.
[14] M.W. Brumm, H.J. Grabke, Corros. Sci. 33 (1992) 1677–1690.
[15] U. Hemmersmeier, M. Feller-Kniepmeier, Mater. Sci. Eng. A248 (1998) 87–97.